Evaluation of Erosion Reduction Mechanisms in Hall Effect Thrusters

IEPC-2015-280/ISTS-2015-b-280

Presented at Joint Conference of 30th International Symposium on Space Technology and Science, 34th International Electric Propulsion Conference and 6th Nano-satellite Symposium
Hyogo-Kobe, Japan
July 4–10, 2015

D. Pérez-Grande*, P. Fajardo and E. Ahedo†
Aerospace Engineering Group, Universidad Carlos III de Madrid, Spain

A comprehensive evaluation of erosion reduction mechanisms in Hall Effect Thrusters with dielectric walls is performed. Two physical mechanisms: *plasma density reduction at key thruster wall positions* and *acceleration region displacement*, are presented as the main mechanisms which must be exploited in order to achieve reduced thruster wall erosion rates. Initially derived through qualitative conclusions from wall sputtering models, these mechanisms are reviewed against experimental and numerical evidence presented in the existing literature; it is found that other reported mechanisms might be secondary to the ones mentioned and that *plasma lensing* must be achieved to avoid requiring a trade-off between erosion reduction and performance degradation in the thruster. Finally, an in-depth theoretical study is carried out for the basis of these mechanisms, backed by numerical simulations performed using the HallMA code.

I. Introduction

One of the main technological challenges faced by Hall Effect Thrusters (HETs) comes in the form of an operational lifetime limitation due to erosion of the thruster channel walls due to plasma-material interactions. Typical certification values are presently of the order of 10000h, which applies to any device independent of its power-class and is low in comparison to other thrusters, limiting widespread use of HET technology within the space industry.

Degradation in HETs is caused due to high energy ion impacts, responsible for sputtering of wall materials which, eventually, are fully abraded. HET walls are commonly manufactured from dielectric ceramic materials which have low sputtering yields; however, erosion of the thruster walls eventually leads to an exposure of the magnetic material to ion bombardment; this circumstance is generally associated with the end of the thruster's useful life.

The erosion phenomenon in HETs is also partly responsible for limitations to the operational voltage (due to the need to limit the energy of impacting ions) and, as a consequence, to specific impulse (Isp). It is also responsible for blocking attempts at miniaturizing HET technology as the effects of ion bombardment and energy losses to the wall are more severe in smaller devices: HETs with power levels of the order of 100s of Watts are likely to fail after ∼1000h of operation.[2]

Current development in the community is focused on a number of derived and optimized configurations in order to deal with erosion related limitations: a number of laboratory and experimental thrusters have based Erosion Reduction Strategies (ERS) on clever (and sometimes unintentional) modifications to magnetic topologies and thruster geometries that retain the base principles of HETs while greatly reducing thruster erosion: BPT-4000 (Aerojet Rocketdyne), H6MS (JPL), NASA-300MS (NASA Glenn & JPL), WL-HT (ICARE), MIHA (Stanford University) (Section III).

These ERS have gained various technical names: Magnetic Shielding (MS), Magnetic Interference (MI), etc.; the theoretical basis behind them has been greatly discussed, with a number of physical mechanisms

*Correspondence Author @ daperezg@ing.uc3m.es
†Keynote Speaker

standing as the underlying causes, or "first principles" for erosion reduction. However, careful investigation on this matter suggests that only two main physical mechanisms are truly responsible for reduction in erosion rates in any of the surveyed cases.

The goal of this paper is to review the existing ERS in the literature against the previously mentioned "base" physical mechanisms for erosion reduction in HETs, and present numerical simulations which confirm these ideas; simulations are carried out using the HallMa Hybrid-PIC code developed by Escobar & Ahedo[4] on custom configurations of the SPT-100 HET. It is worth noting that reviews and proposals presented here are focused on classical annular HETs with dielectric ceramic walls.

II. Erosion Mechanisms in HETs

A. Generalities

Erosion in the walls of EP thrusters such as HETs, TAL, HEMP of Helicon thursters implies the removal of atoms from a solid's surface by ion bombardment (sputtering). It is a complex and widely studied phenomenon[5–8] that depends on a number of properties of the thruster being studied: wall material, magnetic topology, operating condition, etc. Quantitatively, it is described through the wall recession rate ξ:[8]

$$\xi = \frac{dh}{dt} = g_{iw} \cdot Y(E_i, \theta_i) \tag{1}$$

Where g_{iw} is the ion particle flux to the wall and $Y(E_i, \theta_i)$ is the volumetric sputtering coefficient or sputtering yield of material, which depends on the properties of the wall material itself, the impacting ion energy E_i and the impact incidence angle θ_i. Generally, the particle flux is not mono-energetic and the above equation takes an integral form, but this rigor is not essential for the discussion here. More important is that $Y(E_i, \theta_i)$ is negligible below an Energy Threshold E_{th} (typically in the range 20-40eV -Ref. 3-) and then tends to increase more or less linearly with E_i. Essentially, this leaves two main paths for decreasing the wall erosion rate: to *reduce the energy of the impacting particles* or to *reduce the particle flux to the wall.*

In HETs, ions gain energy through the plasma electric potential drop, biased by the applied discharge potential V_d, and through the potential drop established in the sheath regions close to the walls (typically to satisfy the null-current condition imposed by the dielectric walls). This sheath potential V_{sheath} increases with the local electron temperature T_e[9] and also depends on other, more complex, events such as Secondary Electron Emission (SEE).[10]

These physical effects, neglecting the influence of collisions between ions and heavy species (which have not been taken into account for the sake of simplicity), may be summarized as:

$$g_{iw} \approx n_i \sqrt{\tfrac{E_i}{M_i}} \propto n_e \sqrt{T_e};$$
$$E_i = f(V_{acc});$$
$$V_{acc} = f\{\Delta V_d, V_{sheath}(T_e)\};$$

That is, local ion flux to the wall depends on the ion (plasma) density and the ion velocity. Both ion velocity and ion energy depend on the accumulated potential drop V_{acc} that the ion experiences throughout its trajectory to the wall; this takes into account the potential within the plasma bulk as well as the potential drop developed at the sheath. Considering all of the above, we propose that the base physical mechanisms for ERS are *Plasma Density Reduction* and *Acceleration Region Displacement*: in order to diminish the wall recession rate due to erosion, plasma densities next to the thruster walls need to be kept low and ions must not be subjected to large potential drops before reaching their impact points. The latter implies both ensuring that potential gradients in the plasma do not result in heavily energetic ions colliding with the walls, and that the high T_e sheath regions do not supply additional energy to the bulk of the ion population through high V_{sheath}.

A main concern is how (and if) erosion reduction may be accomplished while retaining reasonable performance values for the thruster, and what level of control we have over the separate effects. Performance values in HETs are described through the total efficiency equation (Eq. (2)[1]):

$$\eta = \frac{T^2}{2\dot{m}_p P_d} \tag{2}$$

However, a "partial efficiency" or "phenomenological" approach may be preferred in order to understand which physical mechanisms are affected by a particular change (Section V, Eq. (11) & (12)).

B. Sputtering Yield Empirical Models

The lack of easily accessible data on sputtering yields for typical HET wall materials for ion impacts with energies typical of the bulk ion population in HETs has favored the use of theoretical based analytical formulas which are fine tuned using available data. Such theoretical models were proposed by Yamamura and Tawara;[5,6] they consist on a "Normal Sputtering Yield" Y_n, calculated for mono-energetic ion beam abrasion, and an adjusted "Angular Sputtering Yield" Y_θ which factors the effects of impacts at an angle.

Cheng and Martinez-Sanchez[8] found a "best-fit" for the Normal Yield and Angular Yield expressions based on the data by Yalin[7] for the BN wall material used in the BHT-200 HET (BUSEK Space Propulsion Systems); these models have proven to offer good prediction of erosion effects[31] and are used in the simulation results presented in Section V:

$$Y_n(E) = \frac{AE^{0.474}}{1+BE^{0.3}}\left(1-\sqrt{\frac{E_{th}}{E}}\right)^{2.5} \tag{3}$$

Where A and B are experimentally adjusted coefficients that depend on the Energy Threshold E_{th}, below which sputtering is negligible; for a E_{th}=30eV, $A = 3.20828 \cdot 10^{-4}$ and $B = -0.139106$.

$$Y(Y_n, E, \theta_i) = Y_n \cdot Y_\theta = Y_n \cdot \cos^{-F}(\theta_i) \cdot e^G \tag{4}$$

$$F = f\left(1 + 2.5\frac{aE^{-0.5}}{1-aE^{-0.5}}\right); \quad G = -\Sigma\left(\frac{1}{cos(\theta_i)} - 1\right)$$

Where $f = 5.97563$, $a = -3.63786$ and $\Sigma = 1.41355$. The exactness of the theoretical model against experimental data may be found in Ref. 8.

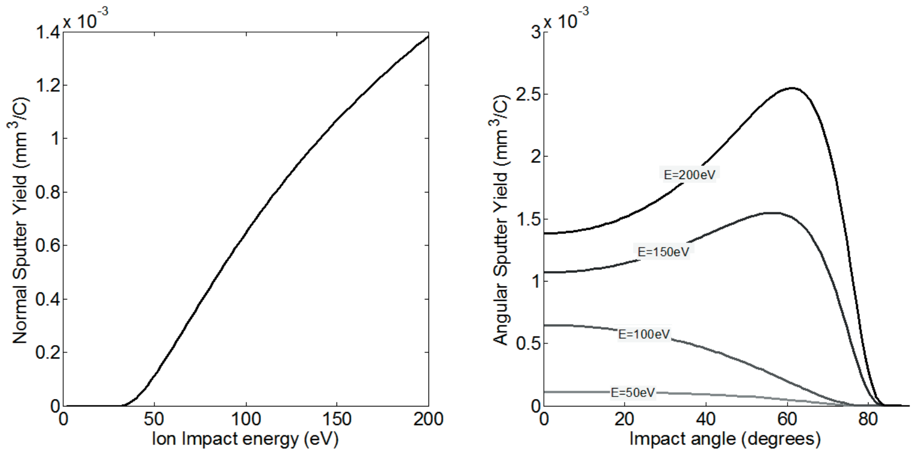

Figure 1. Fitted curves for Normal and Angular Sputtering Yields ($E_{th} = 30eV$)

It is worth noting that E_{th} is responsible for the lack of erosion typically seen on the back region of annular HETs (close to the propellant feed); its effect over the sputtering yield somewhat modifies the understanding of ERS based on reducing the particle flux to the wall, as this is only required in regions where ions have attained energies higher than E_{th} (typically, closer to the thruster exit).

III. Experimental and Theoretical Evidence for Erosion Reduction Strategies

This Section reviews the physical mechanisms and performances of various relevant examples of experimental and theoretical evidence which might be found in the literature on HET erosion reduction. The concepts introduced here are further discussed in Sections V and VI.

A. BPT-4000

Aerojet's BPT-4000 (now XR-5), as reported by deGrys,[11] showed no measurable signs of erosion on the insulator ring (i.e., the thruster channel walls) between 6,700 and 10,400 operation hours during qualification testing of the thruster.

This test revealed that there were yet unexplored design opportunities to greatly reduce HET erosion; because of the nature of the test, it was clear that a fortunate combination of the magnetic topology and the End Of Life (EOL) channel geometry were responsible for the "zero erosion" state.

The physical mechanisms behind this achievement were reviewed by Mikellides et al.:[12] the term *Magnetic Shielding (MS)* was coined to refer to the combination of local magnetic topology, sheath physics and two-dimensional plasma potential distribution effects leading to the reduction of erosion (refer to Section III.C for further examples of MS).

The discussion on MS is centered on *which* magnetic field lines "graze" the walls of the thruster. Indeed, a typical assumption in HETs, due to the high anisotropy imposed by the confining magnetic field, is that magnetic field lines are isothermal on T_e; i.e., in the direction parallel ($\|$) to the magnetic field:

$$\nabla_{\|} T_e \approx 0 \tag{5}$$

This *isothermality* leads to a "reduced" expression for the electron momentum equation *along magnetic field lines* known as the Maxwell-Boltzmann equilibrium law or "thermalized potential relation":

$$\phi = \phi_0 + T_{e,0} \cdot ln\left(\frac{n_e}{n_{e,0}}\right) \tag{6}$$

Where $n_{e,0}$, $T_{e,0}$ (the isothermal magnetic field line temperature) and ϕ_0 (the thermalized potential) are constants for each magnetic field line.

The MS theory proposes that as long as the magnetic field lines reaching or grazing the thruster walls have sufficiently low T_e, the potential drop along them will be negligible, thus impeding the ions from acquiring significant energies before reaching the walls. In addition, low T_e field lines have the advantage of providing sheaths with reduced potential falls to the wall, further diminishing the total ion impact energy.

In the case of the BPT-4000, the conclusion reached was that the EOL configuration "revealed" a magnetic topology which led to low temperature lines reaching the exit of the thruster channel, the consequences being the reduction of both ion energy and ion fluxes to the walls and reduced erosion.

In order to discuss if MS theory is sufficient to justify erosion reduction, we would like to focus on the simulation results shown in Ref. 12 (specifically on the figures presenting the axilsymmetric plasma profiles[a]), which compare the simulated plasma discharge profiles for two geometries of the thruster channel: one which takes into account the erosion produced after 1200hrs of operation, and one which represents the steady-state (EOL) "zero erosion" configuration: these results showcase the downstream displacement of the acceleration region (marked by the zone with large $\nabla\phi$) in regards to the thruster geometry and on the reduction of plasma density along the chamfered region.

To conclude, some performance data may be extracted from Ref. 11; for the 300V discharge potential (V_d) configuration there is an initial reduction of ~4% in thrust during the first ~1500hrs of operation (which coincides with the harshest erosion regime in the operation of the thruster). Because no data is shown in regards to variations in discharge current, the discharge electric power (P_d) is assumed to remain constant through operation. Using Eq. (2), we estimate that *the thruster experienced at least a 7.4% degradation in performance* due to effects related to erosion in the thruster walls, as we expect (based on our own results shown in Section V.B.2) that the discharge power would have likely increased.

B. WL-HT & MIHA

The Wall-Less Hall Thruster (WL-HT) developed by Mazouffre[13] and the linear HET Magnetic Interference Hall Accelerator (MIHA) developed by Thomas[14] are two widely different HETs which, incidentally, utilize

[a]Fig. 13 in Ref. 12

the same approach towards erosion reduction in the thruster walls: to *shift the acceleration, and possibly ionization, regions outside of the thruster channel.*

A self-localized electric field (biased by the imposed discharge potential) exists in the plasma to accelerate the ion population; the position of the acceleration region will be determined by complex interdependencies given by the governing physical mechanisms, however, it is sufficient to know that the magnetic topology and, specifically, the relative location of the magnetic field intensity peak, will play a predominant role.

In the WL-HT, the positioning of the electric potential drop is determined by both the magnetic field peaking, and the anode being located (through a conducting ring with the biased anode potential), at the thruster exit. In the MIHA, the electric potential drop is tuned through two distinct anode positions and various configurations of magnetic field coils. Erosion results for both thrusters are not shown, but concluding comments indicate that reduction in erosion rates is expected for both cases due to the shift in the electric potential drop. Additionally, it is implied that this strategy may open up a design opportunity for shortening the thruster channel length.

Performance wise, Mazouffre points out the deteriorated performances of the WL-HT vs. the un-modified version of the thruster. Some relevant information on performance degradation might be extracted from Ref. 13: for $V_d = 200V$ and $\dot{m}_p = 1mg/s$ case, there is an increase in discharge current from $0.89A$ to $1.05A$ when going from the un-modified thruster to the WL version; additionally, if we take the most probable ion velocity as an indicator for the thruster Specific Impulse (I_{sp}), we gather that the I_{sp} drops from $15200m/s$ to $13510m/s$ (the ratio between the two may be translated directly to a thrust loss ratio, as $I_{sp} = \frac{T}{\dot{m}_p}$).

Again, utilizing Eq. (2) we obtain that *the thruster experienced an estimated ~33% degradation in performance* when the WL modifications were in place. In the case of the MIHA literature, no performance indicators are offered, although comparison to a conventional annular HET might have proven difficult due to its linear configuration.

C. MS thrusters: H6MS, NASA300-MS, MaSMi

High specific impulse and high efficiency HETs have been typically tied to *higher Discharge Voltages* and a magnetic topology which favors a *plasma lensing effect*, as concluded by Hofer.[15] Of course, higher I_{sp} & V_d devices will produce more energetic ion populations which, in turn, require careful consideration of erosion in the thruster. The H6MS,[16] the NASA300-MS[17] and the MaSMi[2] are examples by NASA and JPL of highly efficient thrusters which are aided by the reduction of erosion through the MS ERS.

The best description of the MS physical effect is given by Mikellides;[18] MS thrusters consist of a channel which ends in a chamfered region and a magnetic topology that produces magnetic field lines that are concave in the axial direction (Fig. 2). The magnetic field lines "graze" the thruster walls and, additionally, define a "magnetic lens".[19]

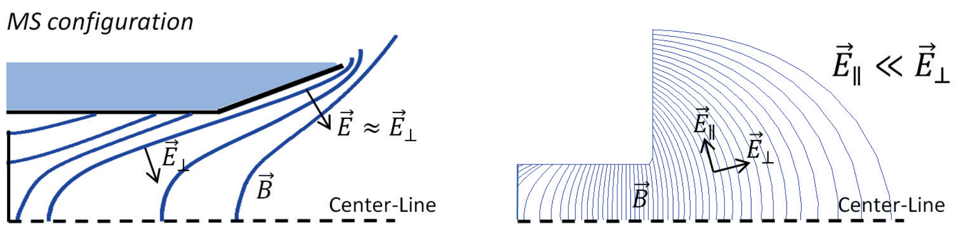

Figure 2. MS configuration by Mikellides et al.[18] (left); typical (un-shielded) configuration in HETs -SPT-100- (right)

MS is based, as per Eq. (5) and (6), on the isothermality of magnetic field lines and on the possibility of them being nearly *isopotential* under certain conditions: low variation of plasma density along the line and/or low T_e in the line. In the H6MS and the NASA-300MS, the magnetic topology and plasma profile are such that the electric field parallel to the lines ($E_\parallel = \nabla_\parallel \phi \approx 0$) is small for most part of the discharge and the electric field generated is mostly perpendicular ($|\vec{E}| \approx E_\perp$) to the lines; because of the concave nature of the lines, this favored $E_\perp$ directs ions away from the walls of the thruster channel.

It is worth noting that, whatever the magnetic topology, the immediate area next to the wall can never present the electric field configuration shown in Fig. 2(left) due to the Bohm ion-kinetic condition and the sheath potential drop, which implies ions being accelerated toward the walls.

Additionally, the concave magnetic field lines allow for the plasma lensing effect to be achieved: reportedly, this is one the reasons behind the high efficiency regimes in these thrusters, as the magnetic lens generates a highly collimated ion beam.

The MS configuration is responsible for the erosion reduction: experimental and simulation results show that the MS versions of the H6 and NASA-300 thrusters attain a *reduction of ∼3 orders of magnitude in erosion rates* as compared to the "un-shielded" (US) versions (for accumulated testing times of ∼100hrs).

Changes on the plasma discharge profiles due to the MS ERS (results shown in Ref. 17 and Ref. 18) [b] and Fig. 2 in Ref. 18) are the, now familiar, displacement of the acceleration region with regards to the thruster geometry is present in the simulation results of both the H6MS and the NASA-300MS. Additionally, the NASA-300MS reuslts show that the magnetic field intensity peak has been shifted downstream (presumably dragging the acceleration region with it); a similar conclusion may be drawn from the results shown for T_e in the H6MS, as the peak in electron temperature (which is generally located in close proximity of the magnetic field peak) is also shifted downstream.

Finally, performance wise, both thrusters distance themselves from other devices reviewed here: efficiencies in the MS thrusters are consistently >60% (reaching values as high as 70%). Moreover, the introduction of the MS topology and geometry has very little effect over the performance of both devices: *in the NASA-300MS the performance degradation is of the order of 4%* as compared to the US NASA-300*; for the H6MS the performance loss is of the order of 3%* compared to the US H6 (according to data presented by Snyder[24])

It is worth noting that the channel length in the NASA-300MS was shortened with no appreciable changes in the thruster performances;[17] this suggests that an additional improvement over thruster weight economy might be gained from the physical effects discussed here.

IV. Base Erosion Reduction Mechanisms

A. Density reduction at key thruster wall positions

Eq. (1) and the physical relations for HETs shown in Section II.A show that reducing the plasma (ion) density $n_{i,c}$ is desirable in order to achieve a reduction in erosion. For a typical anular HET, the plasma density may be easily altered by changing the cross section of the thruster (∼ height × diameter):

$$\dot{m}_i = n_i m_i v_i A \rightarrow A = \pi(h \times d) \propto \frac{\dot{m}_i}{n_i} \tag{7}$$

At typical propellant utilization efficiencies in HETs, the $\dot{m}_i$ is relatively fixed and thus, Eq. (7), shows how the cross section may be used to alter plasma density. However, scaling methodologies for HETs proposed in the literature (Misuri,[20] Dannenmayer,[21,22] Ahedo[23]) indicate that a critical propellant (neutral) density is required for correct operation of the thruster; this density will also be affected by changes in the cross section. In order to avoid altering the operation of the thruster while attempting to reduce erosion, we may consider the effects of the E_{th} in the sputtering yield: it is not necessary to reduce plasma density throughout the thruster, but only in those regions where high energy ions might impact the walls. In a conventional HET configuration, these regions are the thruster channel exits, where a chamfer in the geometry (such as the one presented in the H6MS, the NASA-300MS and even in the BPT-4000) allows for local plasma density reduction and, thus, a reduction in the erosion rate; this is corroborated by the simulation results presented in Section V.B.2.

An additional argument is that, as in the WL-HT configuration, chamfering of the thruster walls might not be required as a means to achieve erosion reduction if the bulk electric potential drop is situated strictly outside of the thruster channel (as suggested by the simulation results presented in Section V.B.3).

[b] Fig. 3 and 4 in Ref. 17

B. Acceleration region displacement

As can be implied from previous arguments, the displacement of the acceleration region downstream from the thruster exit must constitute a reason for erosion rate reduction in the thruster, as ions will not attain enough energy to cause damage to the ceramic walls until after they have cleared the thruster channel.

It is understood that the design of the magnetic topology is paramount in locating the acceleration region; its position is generally associated with areas of high electron resistivity in the plasma discharge. This being said, the exact location of this region is difficult to predict without recurring to numerical simulations and/or experimental set-ups; more so because it will greatly depend on the operational parameters of the discharge.

Modeling of the electron population in the plasma discharge of HETs is typically done under the assumption that it is a Maxwellian fluid of a highly anisotropic nature (caused by magnetic confinement). The fluid description follows a "perturbed 1D" model which is described in detail by Escobar in Ref. 4; the system of equations is solved for the evolution of the electron temperature T_e, the thermalized potential ϕ_0 from Eq. (6) and the total electron current I_e crossing the magnetic field lines on its way from cathode to anode.

The acceleration region is self-localized by the plasma based mainly on the local confinement, in which the magnetic field, the electron density and temperature, and other effects related to electron transport (such as instabilities in the plasma), play a role. Typically, the region with the highest gradient of ϕ_0 determines the acceleration region and is established closely to the magnetic field intensity peak, which generally also coincides with the peak T_e region.

Modifying the magnetic topology of the thruster will have a direct effect over the location of the acceleration region; it is in these cases where HET plasma discharge simulations become valuable to explore optimization and configuration opportunities in conventional thrusters. Indeed, in a conventional HET, due to the magnetic circuit design, the peak magnetic field is inside the thruster channel or very near its exit; the resulting electric field guarantees that high-energy ions will impact the channel wall, limiting the operational life of the thruster. This may help to understand why the magnetic topology utilized in thrusters such as the MIHA or the H6MS and NASA-300MS favors an external acceleration region.

C. *Further discussion*

1. *Discussion on Magnetic Shielding "grazing line" theory*

The use of the "grazing line" theory in a plasma which presents isothermality and quasi-isopotential magnetic field lines is used as a physical basis for the MS ERS. The theory implies that the $E_\perp$ in the concave magnetic field is dominant and reduces the ion impact energy to the walls.

In oder to understand whether this is the main effect for erosion reduction, we perform a simple qualitative analysis on the opposite problem: an "un-shielded" configuration; let us take the results from the *magnetically un-shielded* SPT-100 configuration, from the simulations presented in Section V.B.1, as a representative case (Fig. 3).

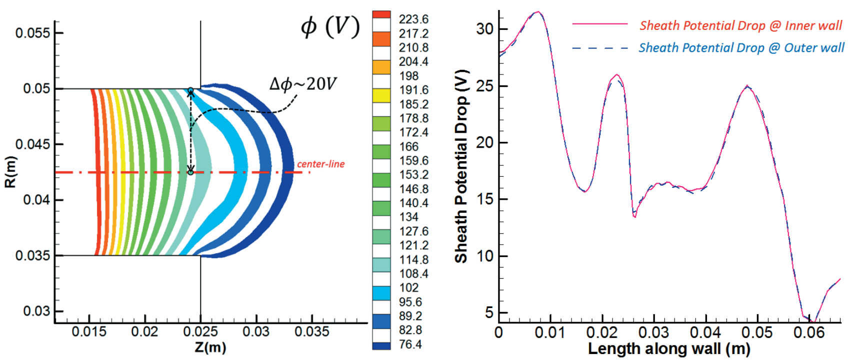

Figure 3. Detail of radial Electric Potential drop @ thruster exit in Base simulation, zebra striped for clarification (left); Sheath potential drop established at the walls (right)

For the $V_d = 300V$ discharge, the radial bulk potential drop within the thruster channel region is of the order of ∼20V and the sheath potential drop accounts for an additional ∼20V, this means that the radial (or normal-to-the-wall) ion energy must be of the order of 40eV (a similar value to the E_{th} -Ref. 3-). In comparison, a typical value for ion axial energies under the given discharge potential would be of the order of ∼100eV (as the discharge potential only translates partially into the final ion kinetic energy due to the various loss mechanisms).

We can conclude that, without the bulk potential drop occurring before the impact (within the channel), ions would barely cross the sputtering threshold E_{th}. We propose that this is also the case in the "MS configuration": the erosion reduction effect may be explained through the *acceleration region displacement* and *density reduction* mechanisms, of which experimental and numerical evidence has already been given in Section III.C.

2. *Clarification on magnetic lensing*

The main challenge presented by ERS is to reduce erosion rates in HETs without affecting performances and/or operation in the thruster. This is evidenced by the experimental results for the WL-HT or the BPT-4000, in which thruster efficiency takes a toll in exchange for longer thruster operational lifetimes allowed by reduced erosion; similar results in terms of performance degradation may be found in the simulation results presented in Section V. An exception to this would be the results shown for the MS thrusters (Section III.C), in which consistently high efficiencies are obtained with little-to-none performance degradation caused by changes in the magnetic topology between the US and the MS versions. Hofer[15] ties these effects to a favorable scaling of thruster efficiencies with increasing Discharge Voltages and to the magnetic lensing topology.

Plasma lensing is considered paramount in retaining acceptable efficiency values once the acceleration region has been shifted downstream from the thruster channel exit. This requirement may be understood by comparing simulation results for the H6MS and the NASA-300MS to our own simulation results for a custom SPT-100 configuration (Fig. 7 and 9): in our custom configuration, the electric field shows high radial curvature and a "fanned out" topology in both Sections V.B.2 and V.B.3, which in turn is partly responsible for a reduction in overall performance due to plume divergence (lower η_{plume}, refer to Eq. (12)).

Comparison of both results also leads to a secondary conclusion: considering the Maxwell-Boltzmann relation (Eq. (6)), because the bulk electric potential drop is established in the vicinity of the peak temperature region, the plasma lensing, which depends on the electric field "following" the concave magnetic field (i.e., having quasi-isopotential lines), can only occur if the density parallel gradients in such a region are sufficiently small. This means that *an external acceleration region also favors magnetic lensing*, as the density gradients are typically smaller downstream from the ionization region (which is generally near the back of the thruster channel).

V. HET Modeling and Simulation Results

In order to complete the evaluation on ERS, a number of simulations have been carried out with the intention of showcasing the two main erosion reduction mechanisms proposed: density reduction and acceleration region displacement. The simulations have been performed using the HallMA code on the SPT-100 magnetic topology; thruster geometry and magnetic field intensity have been customized in order to understand both strategies separately. Wall recession rates are obtained as described in Section II.A.

A. HallMA simulation code and models

The HallMA code (Ahedo & Escobar[4]) is a recent iteration in the development of hybrid -particle/fluid- HET simulation codes that was started by Fife[25] with the well known HPHall, and continued with HPHall-2 (based on the work by Parra & Ahedo[26–29]). Specifically, HallMA integrates the "perturbed" 1D axilsymmetric fluid model for electrons (described in Section IV.B) under a quasi-neutral plasma approximation, with a detailed treatment of plasma-wall interaction through the sheath's physics, both for dielectric and metallic walls. It retains the particle approach to the heavy species while reducing numerical noise and statistical fluctuations through a series of well-proven strategies.

A limitation appears in HallMA because of the lack of theoretical modeling behind certain phenomena in HETs: non-local, non-classical, electron transport along magnetic field lines, plasma turbulent transport, plasma instabilities, etc. This inconsistency is solved in the electron model through a phenomenological approach towards electron perpendicular transport by utilizing the *effective electron collision frequency* ν_e^* :

$$\nu_e^* \approx (\nu_{en} + \nu_{wall}) + \alpha_{turb}\omega_{c,e} \tag{8}$$

Where we can define the terms as:

ν_{en} Electron collision frequency with neutral atoms (collisions with ions are typically negligible), responsible for cross-magnetic-field transport in "classical" terms

ν_{wall} Wall transport coefficient appearing due to the existence of plasma-wall interaction (namely due to unmagnetized secondary electrons and diffusively backscattered primary electrons)

α_{turb} Turbulence parameter: a relative measure of plasma turbulent transport, which is scaled to the electron cyclotron frequency ($\omega_{c,e}$).

In principle, α_{turb} can be considered to englobe the effects of azimuthal instabilities in the plasma which give rise to a non-null forcing term in the electron momentum equation, contributing to electron transport. Typical values in the literature are the classical Bohm value of $\alpha_{turb} \sim 1/16$ or values proposed by Fife[25] and Ahedo[30] of $\alpha_{turb} \sim 1/100$; effectively, α_{turb} is an additional degree of freedom in our problem which we adjust to fit simulations to experimental results. The influence of ν_e^* appears through the effective Hall parameter, which is a fundamental part of the electron transport equations:

$$\beta_e^* = \frac{eB}{m_e \nu_e^*} \tag{9}$$

The magnetic field affects the discharge only through the effective Hall parameter β_e^*; this may be compared to a "classical" Hall parameter, $\beta_{en} = \frac{eB}{m_e \nu_{en}}$, which only takes into account the collisional transport. Turbulent transport may be then understood to affect the effective confinement of the magnetic field, represented by an effective magnetic field intensity B^*, which may be proven to satisfy:

$$\frac{eB}{m_e \nu_e^*} = \frac{eB^*}{m_e \hat{\nu}_{en}} \rightarrow \frac{B^*}{B} = \frac{1}{1 + \alpha_{turb}\beta_{en}} \tag{10}$$

That is, an electron population with turbulent transport modes and a magnetic field intensity B is subjected to magnetic confinement in the same way as one in which only collisional transport modes are considered but is magnetized by a field of intensity B^*; while α_{turb} is a parameter inputted by the user in the simulation, β_{en} actually depends on the simulation results through the collisional frequency $\nu_{en} = \nu_{en}(n_n, n_e, T_e)$. This concept of effective magnetic field will be of use in Section V.B.

B. Simulation results

1. *Base SPT-100 configuration*

A base SPT-100 magnetic topology and thruster geometry has been simulated with the intent of acting as a reference for the simulations showcasing ERS, also presented in this section. Moreover, the simulation was used for adjusting the turbulent transport parameter α_{turb} to achieve results which are comparable to experimental results for the SPT-100, specifically to those published by Sankovic.[32]

The SPT-100 is characterized by a straight thruster channel and a magnetic field topology that is mainly radial and peaks in intensity near the channel exit; the simulation domain, as well as the field topology and intensity are shown in Fig. 4.

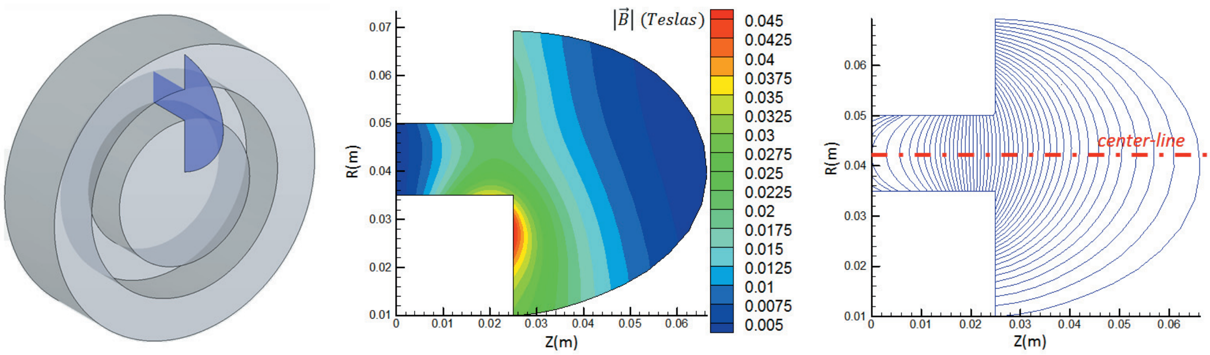

Figure 4. Simulation Domain on a 3D SPT-100 geometry (left); Magnetic Field Intensity in simulation (center); Magnetic Field line topology (right)

A parametric search on the turbulent parameter space and previous experience of typical in-simulation values allow us to obtain reasonably well adjusted results for the base simulation; Table 1 compares thruster performance values and efficiencies for the simulated case and the experimental values given by Sankovic.

	Simulation (Base)	Experimental	$\triangle(\%)$
$V_d(V)$	300	299	$\sim$
$I_d(A)$	4.2	4.5	-6.6
$P_d(W)$	1262	1350	-6.6
$\dot{m}_{prop}(^{mg}/_{s})$	5	5.18	-3.6
$T(mN)$	78	82.7	-5.6
$I_{sp}(s)$	1570	1550	+1.3
η_T	0.48	0.46	+3.2
η_{plume}	0.91	-	-
η_u	0.79	-	-
η_c	0.78	-	-
η_v	0.77	-	-

Table 1. Base Simulation results vs. Experimental values

The performances shown here attend to a phenomenological thruster performance model:

$$\eta_t = \eta_v \eta_{plume} \eta_c \eta_u \eta_q \tag{11}$$

Where the partial efficiencies are defined as:

$$\eta_{plume} = \frac{\langle v_{i,z}^2 \rangle_{S\infty}}{\langle v_i^2 \rangle_{S\infty}}; \eta_u = \frac{\langle \dot{m}_i \rangle_{S\infty}}{\dot{m}_{prop}}; \eta_{curr} = \frac{V_d \cdot \langle I_{d,i} \rangle_{S\infty}}{P_d}; \eta_v = \frac{\langle \dot{m}_i \rangle_{S\infty} \cdot \langle v_i^2 \rangle_{S\infty}}{V_d \cdot \langle I_{d,i} \rangle_{S\infty}} \tag{12}$$

S_∞ represents an area well downstream from the thruster. The dependency of the turbulence parameter $\alpha_{turb}(z)$ with the axial coordinate (Z) is shown in Fig. 5, which also showcases the various magnetic fields to take into account when analyzing the simulations: the magnetic field line along the center-line of the thruster, the mean magnetic field strenght averaged over the field lines and the "Effective Magnetic Field" intensity, as defined by the relation presented in Eq. (10). The averaged magnetic field is more consistent with the actual confinement experienced by electrons, as the 1D model equations take average values over each field line; this concept is important to explain why "portions of the magnetic field, buried into the dielectric material in the BOL design of the thruster" [c] can induce changes in the plasma when the material is eroded. Additionally, it is clear from this figure that the turbulent transport is the dominating term throughout the discharge.

[c]Quoted from Ref. 12

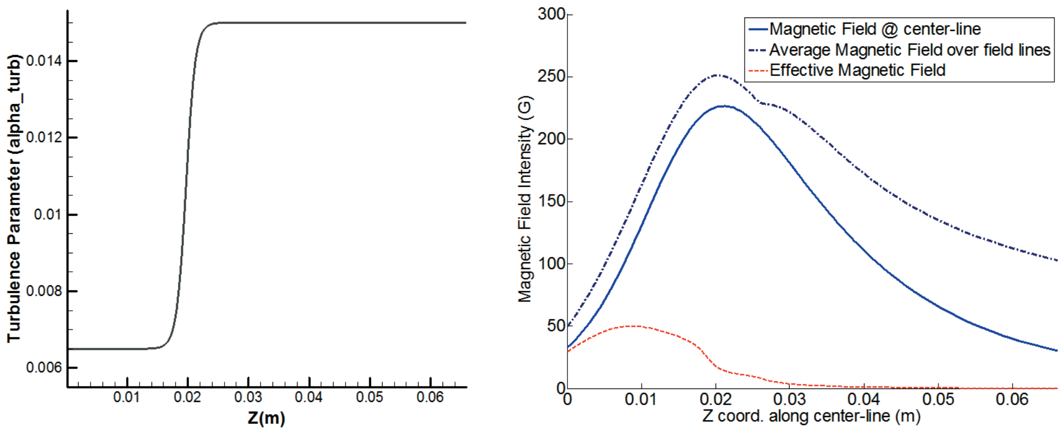

Figure 5. Turbulence Parameter in simulation (left); Average, Center-line and Effective magnetic fields (right)

The base plasma profiles and wall recession rates are presented in comparison to other simulations over the following sections. Erosion statistics are given in Table 2; it is clear that erosion rates are highly aggressive; projecting these rates throughout a typical thruster lifetime of 10,000 hrs, the total abrasion would amount to $\sim 100mm$ of wall material at the thruster exit. The two channel walls experience slightly different recession rates; this is due to slight asymmetries in the plasma profiles with regards to the center-line.

	Base Simulation
Peak Erosion - inner ($^{mm}/_{100h}$)	0.664
Average Erosion - inner ($^{mm}/_{100h}$)	0.103
Peak Erosion - outer ($^{mm}/_{100h}$)	1.05
Average Erosion - outer ($^{mm}/_{100h}$)	0.149

Table 2. Summary on Base simulation erosion results (peak and average values)

2. Chamfered Geometry configuration: Plasma Density Reduction

The effect of denisty on erosion reduction in HET simulations is shown here. For this, the baseline magnetic field topology from the SPT-100 is kept, but the thruster geometry is modified to accomodate a chamfered region corresponding to the erosion peak as shown in Fig. 8. Incidentally, this configuration is reminiscent of the BPT-4000 EOL geometry and will indeed exhibit a reduction in wall recession rates.

The axial profile for the turbulence parameter has also been obtained from the base simulation (shown in Fig. 5), lacking a better approach towards determining it; the chamfered thruster geometry, magnetic field intensity and characteristic magnetic fields are shown in Fig. 6: it is evidenced by the averaged magnetic field that the chamfered geometry reveals a region of the magnetic topology which is closer to the magnetic poles and thus counts with a higher field intensity.

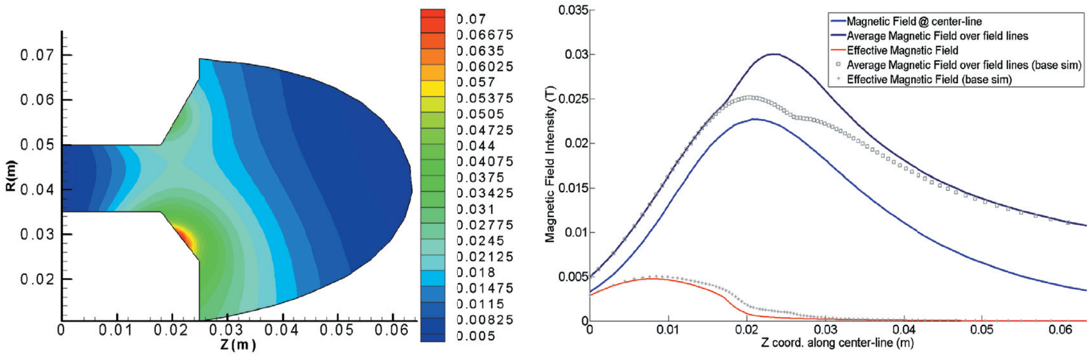

Figure 6. Chamfered Geometry & Magnetic Field Intensity in simulation (left); Average, Center-line and Effective magnetic fields in chamfered geometry vs. base simulation (right)

The performance results obtained from this simulation are shown in comparison to the base case in Table 3. The most obvious contrast is the general drop in the thruster's performance; the reduction in thrust is comparable to the one experienced by the BPT-4000 (refer to Section III.A) and is quite possibly directly tied to a higher plume divergence (lower η_{plume}). Additionally, the thruster establishes an increased discharge current to operate, which is mainly an electron current (explaining the drop in η_{curr}); this leads to a larger discharge power, which, together with the reduced thrust takes a large toll on the overall performance.

	Chamfered geom. sim.	Base sim.	$\triangle(\%)$
$V_d(V)$	300	300	$\sim$
$I_d\ (I_{d,i})\ (A)$	4.54 (3.33)	4.2 (3.30)	+8.1 (+0.9)
$P_d(W)$	1362	1262	+8.1
$\dot{m}_{prop}(^{mg}/_{s})$	5	5	$\sim$
$T(mN)$	70.7	78	-9.3
$I_{sp}(s)$	1496	1570	-4.7
η_T	0.37	0.48	-23
η_{plume}	0.85	0.91	-6.6
η_u	0.76	0.79	-3.8
η_c	0.73	0.78	-6.4
η_v	0.75	0.77	-2.6

Table 3. Chamfered geometry simulation results vs. Base simulation results

The plasma profiles in the chamfered geometry are shown in Fig. 7, with 1D averages presented in comparison to the Base configuration results.

The most evident change is the much larger T_e peak, which mainly affects the plasma density n_e in the channel through the ionization rate. The wall densities at the chamfered region (circled region in the figure) experience a large drop: it is mainly due to this density drop, together with the the minor shift in the location of the bulk electric potential drop (as shown in the figure), that the reduction in erosion is achieved.

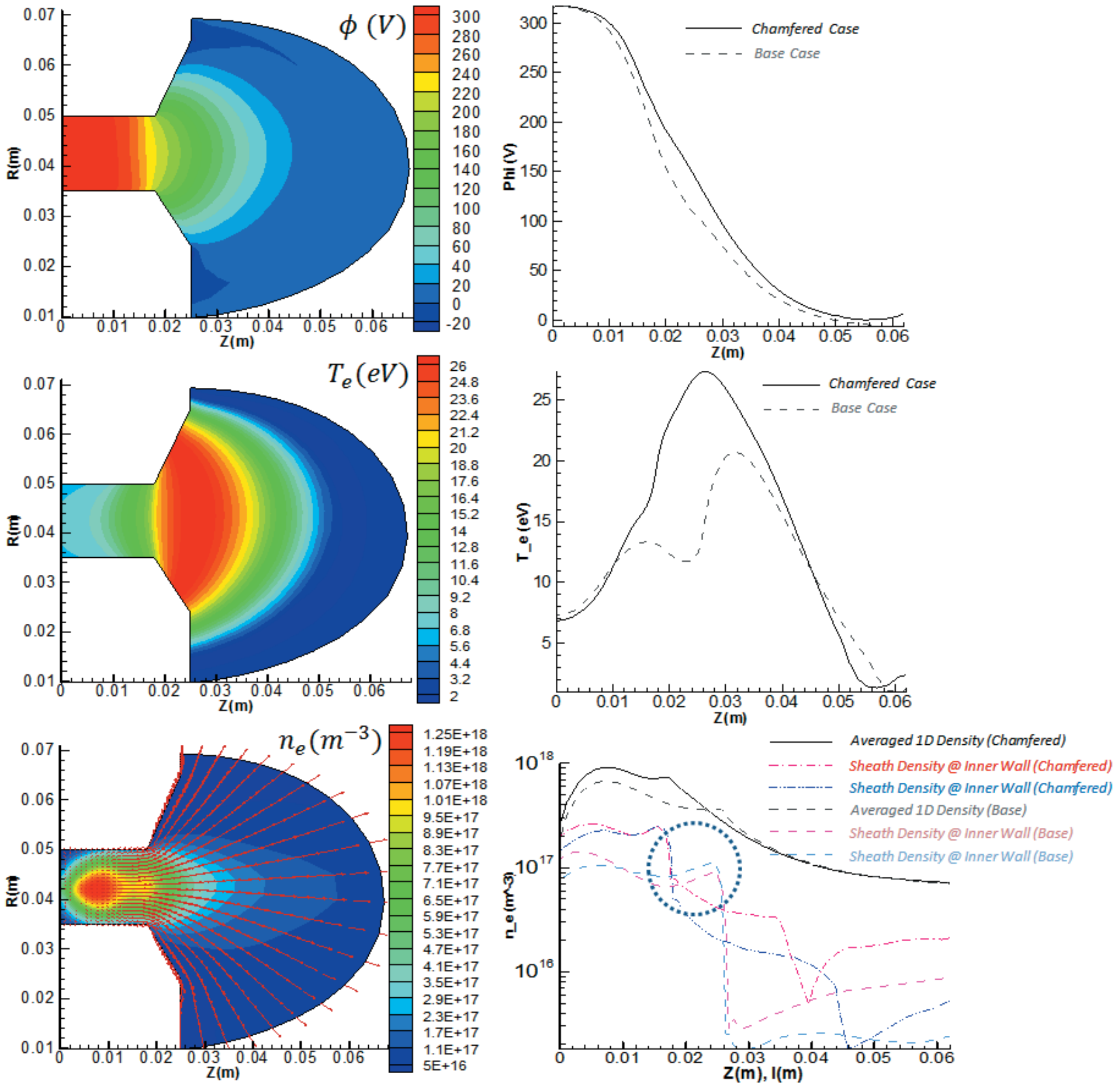

Figure 7. Chamfered Configuration: 2D Plasma profiles in simulation (left) and 1D averages (right). Electric Potential (top); Electron Temperature (middle); Electron Density & Ion Velocity field (bottom). 1D profiles are shown in comparison to base-line simulation

Quantitatively, the results on erosion reduction are presented in Fig. 8 and in Table 4. The change in the thruster's geometry has had a clear effect over the erosion experienced by the walls: while the reduction in wall recession rates by ~ 5 times still far from the 3 orders of magnitude reported in the H6MS and the NASA-300MS (Section III.C), these results cement the idea that an ERS based on plasma density reduction at the thruster exit is an effective strategy and also shed light on why the BPT-4000 experienced its "zero erosion state".

The expected reduction in erosion might be valuable from a design point of view if we consider a trade-off between the performance reduction and the total throughput of the thruster (the total amount of momentum expelled by the thruster through its operational lifetime). Indeed, these results would imply that the operational life-time of the thruster (if we assume that the erosion rate is maintained throughout operation) may be extended by ~ 5 times, which, allowing for the thruster decay and the additional required propellant mass, would report an increase in the total throughput of $\sim 450\%$; this is done at the cost of an increase in discharge power of $\sim 8\%$ in comparison to the Base SPT-100 which must be put in perspective of the total throughput increase.

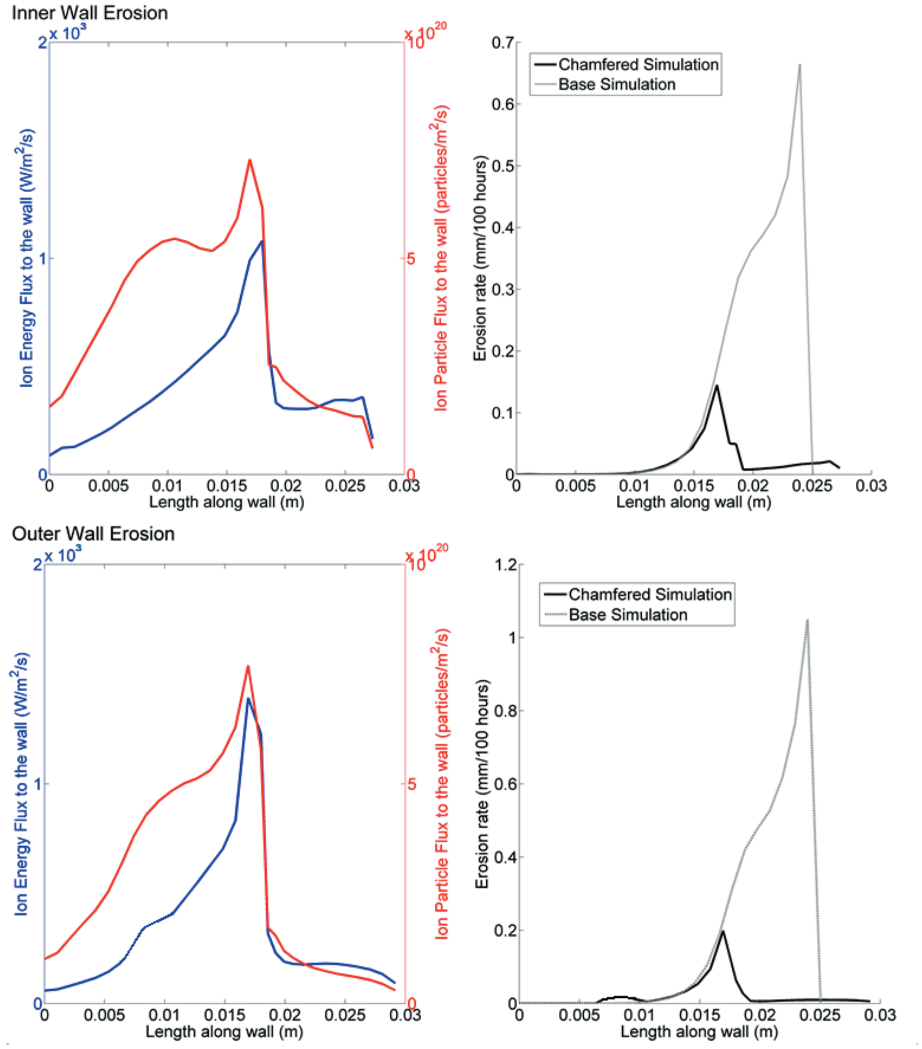

Figure 8. Chamfered Configuration: Inner Wall erosion results (top); Outer Wall erosion results (bottom). Ion particle and energy fluxes to the walls (left); Wall recession rates due to erosion (right) in Chamfered config. vs. Base config.

	Chamfered config. Sim.	Base Sim.	$\triangle(\%)$
Peak Erosion - inner ($^{mm}/_{100h}$)	0.145	0.664	-78
Average Erosion - inner ($^{mm}/_{100h}$)	0.018	0.103	-81
Peak Erosion - outer ($^{mm}/_{100h}$)	0.198	1.05	-82
Average Erosion - outer ($^{mm}/_{100h}$)	0.021	0.149	-86

Table 4. Summary on Chamfered config. simulation erosion results (peak and average values)

3. Theoretical exercise on alternate Magnetic Configuration: Acceleration region displacement

It has been made evident throughout this manuscript, that the magnetic topology in HETs is very much responsible for the resulting profiles of the plasma discharge. While modifying the base SPT-100 magnetic topology is outside of the scope of this paper, a theoretical exercise oriented towards shifting the location of the acceleration region is performed.

Indeed, control over a multiplying factor for the magnetic field intensity and the turbulence parameter allows changing the effective magnetic field in the simulation, in turn altering the plasma profiles. For this section, the base thruster geometry is retained and the magnetic field intensity in the simulated domain is uniformly increased by 20%; the turbulence parameter is modified as shown in Fig. 9 (the resulting characteristic magnetic fields in the simulation are also shown in this figure).

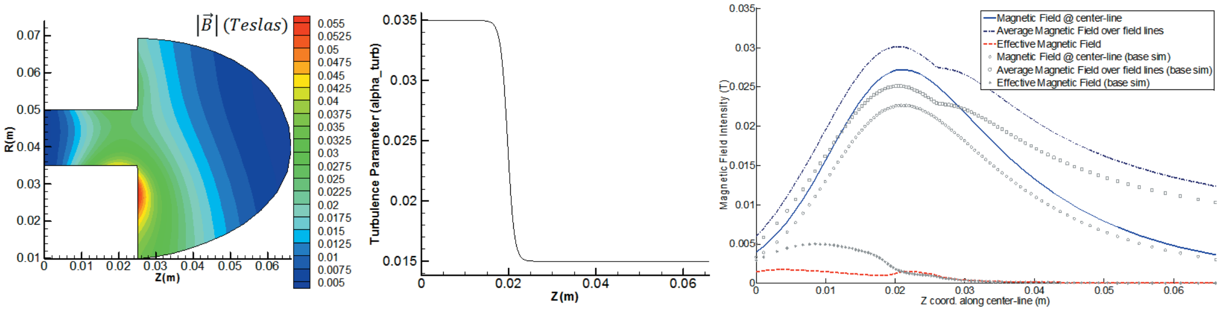

Figure 9. Alt. Magnetic config: Magnetic Field Intensity in simulation (left); Turbulence Parameter in simulation (middle); Average, Center-line and Effective magnetic fields (right)

The effects of this altered magnetic configuration are best understood from the perspective of the effective magnetic field, as a sort of *magnetic screening* of the interior region of the thruster. The authors are aware that the results shown here might not be physically achievable, which is why we consider this to be a more theoretical exercise; however, these results may serve as indication for the effects of shifting the acceleration region downstream in the thruster over performances and plasma profiles, as evidenced in Table 5 and Fig. 10.

	Alt. Magnetic config. sim.	Base sim.	$\triangle(\%)$
$V_d(V)$	300	300	$\sim$
I_d ($I_{d,i}$) (A)	5.15 (3.32)	4.2 (3.30)	+22.6 (+0.6)
$P_d(W)$	1566	1262	+22.6
$\dot{m}_{prop}(^{mg}/_{s})$	5	5	$\sim$
$T(mN)$	75.3	78	-3.4
$I_{sp}(s)$	1474	1570	-6.1
η_T	0.36	0.48	-25.5
η_{plume}	0.80	0.91	-12.1
η_u	0.78	0.79	-1.2
η_c	0.64	0.78	-17.9
η_v	0.79	0.77	+2.6

Table 5. Alternate Magnetic config. simulation results vs. Base simulation results

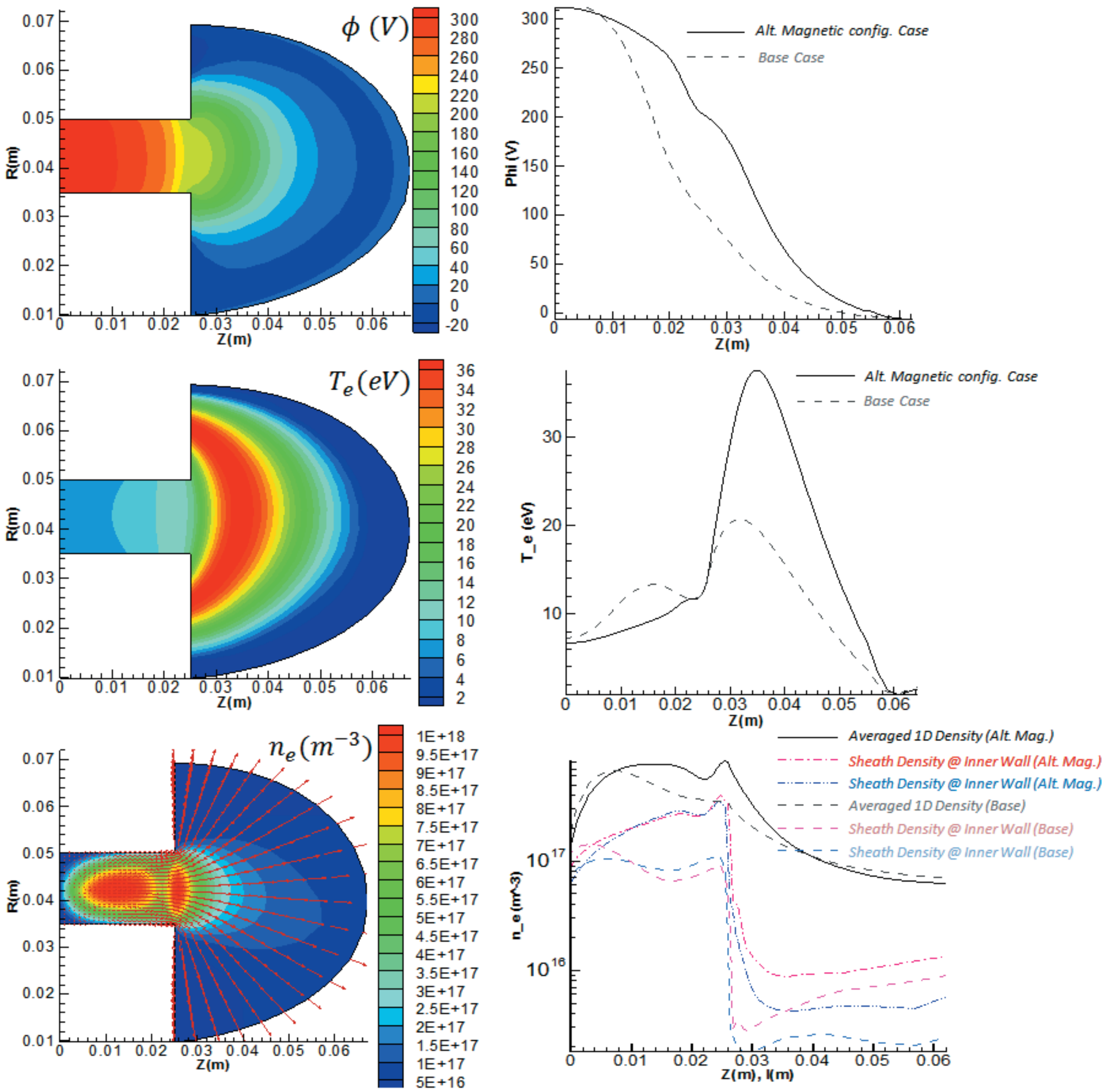

Figure 10. Alt. Magnetic config.: 2D Plasma profiles in simulation (left) and 1D averages (right). Electric Potential (top); Electron Temperature (middle); Electron Density & Ion Velocity field (bottom). 1D profiles are shown in comparison to base-line simulation

The combination of increased magnetic field intensity and the magnetic screening of the back of the thruster produces a distinct T_e profile and the displacement of the acceleration region so that it is mostly external to the thruster; the electron density now showcases a double peak, which revels a secondary ionization region at the thruster exit (undoubtedly because due to the influence of the higher peak electron temperature). Again, the thruster efficiency is reduced due to the lower η_{plume} (plume divergence is increased because of the "fanned-out" profile of the bulk potential drop, heavily influenced by the high magnetic field curvature of the region) and lower η_{curr} (larger electron current required to sustain de discharge); although, the acceleration process is slightly more efficient, as understood from a larger η_{volt} (possibly due to lower ion energy losses in the thruster, a consequence of reduced erosion). It is worth noting that the performance loss in the simulation is comparable to the one experienced by the WL-HT (refer to Section III.B) where an external acceleration region is also enforced.

Wall recession rates are shown in Fig. 11 and Table 5; the results coincide with what is expected given our discussion in Section IV: erosion rates are reduced when the ions are accelerated externally to the thruster, more or less independently of the radial and sheath potential drops within the thruster.

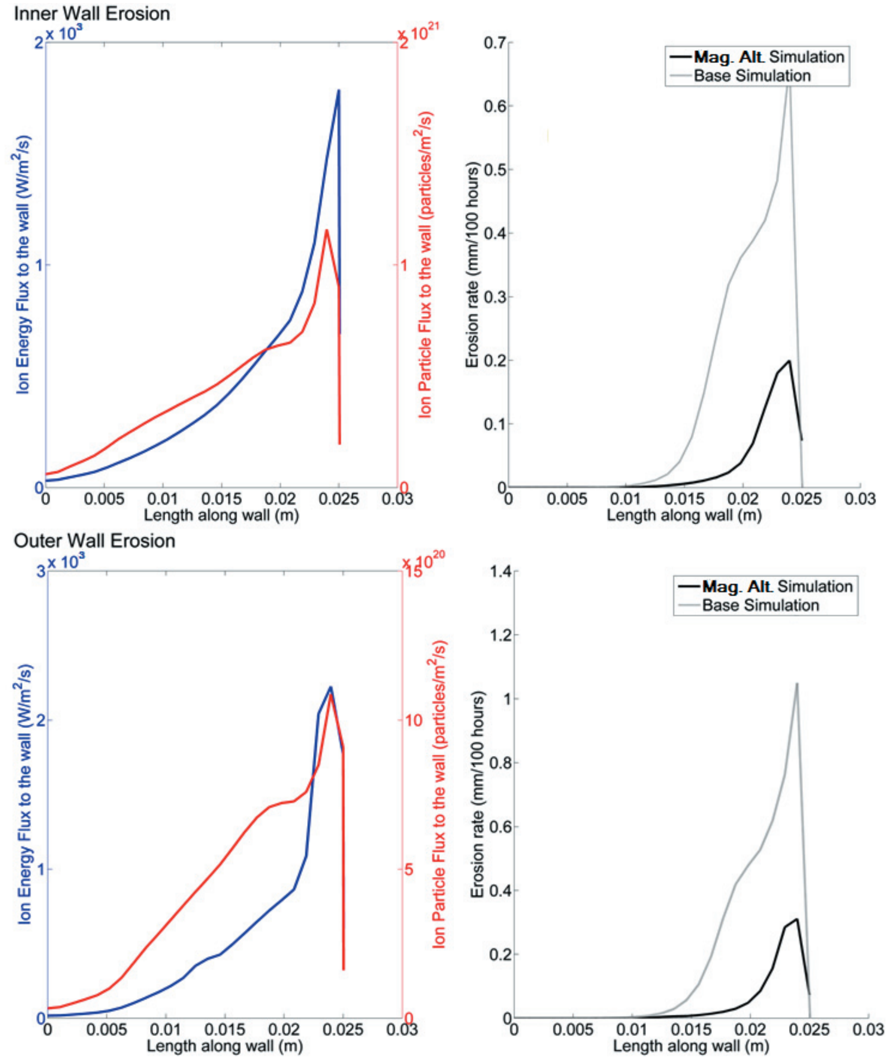

Figure 11. Alt. Magnetic config.: Inner Wall erosion results (top); Outer Wall erosion results (bottom). Ion particle and energy fluxes to the walls (left); Wall recession rates due to erosion (right) in Chamfered config. vs. Base config.

	Chamfered config. Sim.	Base Sim.	$\triangle(\%)$
Peak Erosion - inner ($^{mm}/_{100h}$)	0.199	0.664	-70
Average Erosion - inner ($^{mm}/_{100h}$)	0.03	0.103	-70
Peak Erosion - outer ($^{mm}/_{100h}$)	0.311	1.05	-71
Average Erosion - outer ($^{mm}/_{100h}$)	0.0421	0.149	-72

Table 6. Summary on Alt. Magnetic config. simulation erosion results (peak and average values)

This theoretical exercise has allowed us to test the possibility of altering the magnetic configuration of the SPT-100 in order to determine that an ERS based on acceleration region displacement is indeed and effective strategy. While the particular configuration imposed might not be easily achievable through a combination of coils in the magnetic circuit, our approach for using the turbulence parameter and the magnetic field intensity factor in order to modify the effective magnetic topology could prove to be a "quick research tool" for exploring optimization opportunities in the magnetic topology; e.g., in this case, the same effect could be attained though a magnetic circuit oriented towards increasing the magnetic intensity peak and screening the thruster channel region.

Finally, the authors would like to add that simulations were carried out for this altered magnetic configuration and a thruster channel shortened by 1/5 of its length with no discernible effects over the discharge profiles or wall recession results; this is in line with results for the NASA-300MS.

VI. Conclusions

The on-going discussion regarding the physical mechanisms behind the reduction of erosion rates in HETs has been tackled on a "first principles" basis. Careful review of the theoretical ion bombardment erosion models reveals that only two base mechanisms may exist in reducing erosion: the reduction of ion particle flux to the wall (which may be achieved through a localized reduction of the ion density) and the reduction of the accumulated ion energy before impact (which is achieved by shifting the acceleration region downstream from the thruster).

These base mechanisms are reviewed against the existing literature for HETs, finding that indeed these mechanisms are at play in thrusters in which a reduction of the wall recession rates has been achieved; other proposed mechanisms are either secondary or not "first principles". Magnetic lensing, or Plasma lensing, appeared in the literature as a means to attain high thrust efficiencies when combined with the erosion reduction mechanisms; although it is not strictly necessary for erosion reduction.

Modification of the thruster geometry (by chamfering the annulus exit) and of the magnetic topology in the thruster (oriented toward the shifting of the magnetic field intensity peak downstream from the thruster exit) appear as the natural steps to reduce the wall recession rates. These strategies have been reviewed from a theoretical stand-point and simulations have been carried out to confirm that they are effective in reducing thruster erosion; the simulations are in agreement with what was expected by the authors and with experimental results found in the literature. Furthermore, it was confirmed that if a magnetic lensing topology is not present thruster design will have to trade-off operational lifetime against thruster performance; we assert that, perhaps, this trade-off will be viewed from the perspective of the total throughput capability of the thruster. Additionally, we will also suggest that magnetic lensing topologies lead to narrower acceleration regions (i.e., electric potential drops confined to smaller axial distances) and that this has a positive effect over the efficiency through the partial voltage utilization efficiency.

The intention of the authors is that these base erosion reduction mechanisms may be used as a starting point for future scaling strategies in HET design. Additional work to be carried out would tackle the redesign of the magnetic topology in a theoretical thruster with the intention of achieving a magnetic lensing, erosion reducing, arrangement and exploring the design and operational space opened by this configuration.

The efficiency peak for HETs has still not been reached, and it is precisely the achievement of consistent Erosion Reduction Strategies which will allow us to explore the high Discharge Voltage, high Isp and high efficiency operational regimes without compromising thruster operational lifetimes.

VII. Acknowledgments

This work has been supported by Spain's R&D National Plan, grant number ESP2013-41052-P.

References

[1]Goebel, D. M., and Katz, I., Fundamentals of Electric Propulsion: Ion and Hall Thrusters, JPL Science and Technology Series, Pasadena, CA, 2008, Chapter 7.

[2]Ryan W. Conversano, Dan M. Goebel, Fellow, IEEE, Richard R. Hofer, Taylor S. Matlock, and Richard E. Wirz, "Development and Initial Testing of a Magnetically Shielded Miniature Hall Thruster", IEEE Transactions on Plasma Science, Vol. 43, No.1, January 2015.

[3]Ioannis G. Mikellides, Ira Katz, Richard R. Hofer, Dan M. Goebel, Kristi de Grys, and Alex Mathers, "Magnetic shielding of the channel walls in a Hall plasma accelerator", Physics of Plasmas 18, 2011.

[4]Diego Escobar and Eduardo Ahedo, "Two-Dimensional Electron Model for a Hybrid Code of a Two-Stage Hall Thruster", IEEE Transactions on Plasma Science, Vol. 36, No. 5, October 2008.

[5]Yamamura, Y., and Tawara, H., "Energy Dependence of Ion-Induced Sputtering Yields from Monoatomic Solids at Normal Incidence", Atomic Data and Nuclear Data Tables, Vol. 62, No. 2, March 1996, pp. 149–253.

[6]Yamamura, Y., “An Empirical Formula for Angular Dependence of Sputtering Yields”, Radiation Effects and Defects in Solids, Vol. 80, Nos. 1–2, Feb. 1984, pp. 57–72.

[7]Yalin, A. P., Surla, V., Farnell, C., Butweiller, M., and Williams, J. D., “Sputtering Studies of Multi-Component Materials by Weight Loss and Cavity Ring-Down Spectroscopy”, 42nd AIAA/ASME/SAE/ASEE Joint Propulsion Conference and Exhibit, Sacramento, CA, AIAA Paper 2006-4338, July 2006.

[8]Cheng, S. Y., Martinez-Sanchez, M., “Hybrid Particle-in-Cell Erosion Modeling of Two Hall Thrusters”, Journal of Propulsion and Power, Vol. 24, No. 5, September-October 2008, pp. 987-998.

[9]G. D. Hobbs and J. A. Wesson, Plasma Phys. 9(1), 85–87, 1967.

[10]E. Ahedo and V. De Pablo, “Combined effects of electron partial thermalization and secondary emission in Hall thruster discharges”, Physics of Plasmas 14, 2007.

[11]Kristi de Grys, Alex Mathers, Ben Welander, Vadim Khanyms, “Demonstration of 10,400 Hours of Operation on a 4.5 kW Qualification Model Hall Thruster”, 46th AIAA/ASME/SAE/ASEE Joint Propulsion Conference & Exhibit, AIAA 2010.

[12]Mikellides, I. G., Katz, I., Hofer, R. R., and Goebel, D. M., de Grys, K., and Mathers, A., "Magnetic Shielding of the Channel Walls in a Hall Plasma Accelerator," Physics of Plasmas, Vol. 18, No. 3, 2011, p. 033501.

[13]S. Mazouffre, S. Tsikata, and J. Vaudolon, “Development and experimental characterization of a wall-less Hall thruster”, Journal of Applied Physics 116, 2014.

[14]Cliff Thomas, Emmanuelle Sommier, Nicolas Gascon, and Mark Cappelli, “The Magnetic Interference Hall Accelerator”, 42nd AIAA/ASME/SAE/ASEE Joint Propulsion Conference & Exhibit, July 2006.

[15]Hofer, R. R., "Development and Characterization of High-Efficiency, High-Specific Impulse Xenon Hall Thrusters," Ph.D. Dissertation, Aerospace Engineering, University of Michigan, Ann Arbor, MI, 2004. (Also NASA/CR-2004- 213099)

[16]Richard R. Hofer, Benjamin A. Jorns, James E. Polk, Ioannis G. Mikellides, and John Steven Snyder, “Wear test of a magnetically shielded Hall thruster at 3000 seconds specific impulse”, Presented at the 33rd International Electric Propulsion Conference, October 2013.

[17]Hani Kamhawi, Wensheng Huang, Thomas Haag, Rohit Shastry, George Soulas, Timothy Smith, Ioannis Mikellides and Richard Hofer “Performance and Thermal Characterization of the NASA-300MS 20 kW Hall Effect Thruster”, Presented at the 33rd International Electric Propulsion Conference, October 2013.

[18]Ioannis G. Mikellides, Ira Katz, Richard R. Hofer, and Dan M. Goebel, “Magnetic shielding of walls from the unmagnetized ion beam in a Hall thruster”, Applied Physics Letters 102, 2013.

[19]A. I. Morozov and V. V. Savelyev, Rev. Plasma Phys. 21, 203, 2000.

[20]T. Misuri, F. Battista, and M. Andrenucci, “HET scaling methodology: Improvement and assessment,” in Proc. 44th AIAA/ASME/SAE/ASEE Joint Propulsion Conference, July 2008.

[21]Kathe Dannenmayer and Stephane Mazouffre, “Elementary Scaling Relations for Hall Effect Thrusters”, Journal of Propulsion and Power, Vol. 27, No. 1, 2011.

[22]Dannenmayer, K., and Mazouffre, S., “Sizing of Hall Effect Thrusters with Input Power and Thrust Level: An Empirical Approach,” Journal of Technical Physics, Vol. 49, Nos. 3–4, 2008, pp. 231–254.

[23]E. Ahedo & J.M. Gallardo, "Scaling Down Hall Thrusters", IEPC-2003-104

[24]John Steven Snyder, John R. Brophy, Richard R. Hofer, Dan M. Goebel, and Ira Katz, “Experimental Investigation of a Direct-Drive Hall Thruster and Solar Array System at Power Levels up to 10 kW”, 48th AIAA/ASME/SAE/ASEE Joint Propulsion Conference & Exhibit, 2012

[25]J. M. Fife, “Hybrid-PIC modeling and electrostatic probe survey of Hall thrusters”, Ph.D. dissertation, MIT, Cambridge, MA, 1998.

[26]F. I. Parra, E. Ahedo, J. M. Fife, and M. Martï¿œnez-Sï¿œnchez, “A two dimensional hybrid model of the Hall thruster discharge,” J. Appl. Phys., vol. 100, no. 2, pp. 023 304-1–023 304-11, Jul. 2006.

[27]E. Ahedo, “Presheath/sheath model with secondary electron emission from two parallel walls,” Phys. Plasmas, vol. 9, no. 10, pp. 4340–4347, Oct. 2002.

[28]E. Ahedo, J. M. Gallardo, and M.Martï¿œnez-Sï¿œnchez, “Effects of the radial plasma–wall interaction on the Hall thruster discharge,” Phys. Plasmas, vol. 10, no. 8, pp. 3397–3409, Aug. 2003.

[29]. I. Parra and E. Ahedo, “Fulfillment of the Bohm condition on the HPHall fluid-PIC code,” presented at the 40th Joint Propulsion Conf., Fort Lauderdale, FL, 2004, AIAA 2004-3955.

[30]E. Ahedo, D. Escobar, “Influence of design and operation parameters on Hall thruster performances”, Journal of applied physics 96, 983, 2004.

[31]E. Ahedo, A. Antï¿œn, I. Garmendia, I. Caro and J. Gonzï¿œlez del Amo, “Simulation of wall erosion in Hall thrusters”, IEPC-2007-067

[32]J.M. Sankovic, J.A. Hamley, and T.W. Hang, “Performance evaluation of the russian spt-100 thruster at nasa lerc.” Presented at the 24th International Electric Propulsion Conference, Moscow, Russia, IEPC 93-094. Electric Rocket Propulsion Society, Fairview Park, Ohio, 1993.